








Superhydrophobic Surfaces Based on Nickel Stearate: An Innovative Approach to Coatings on 7050 Aeronautical Aluminum Alloy

Jedaías J. da Silva^{a*} , Ana L. C. Guimarães^b , Walter L. C. da Silva Filho^b ,
Rafael G. C. da Silva^c , Maria I. C. Malta^b , Dayanne D. S. Morais^b ,
Severino L. Urtiga Filho, Magda R. S. Vieira^b 

^aUniversidade Federal de Pernambuco, Programa de Pós-Graduação em Engenharia Aeroespacial, Rua da Inovação, 50740-540, Cidade Universitária, Recife, PE, Brasil.

^bUniversidade Federal de Pernambuco, Departamento de Engenharia Mecânica, Avenida da Arquitetura, 50740-550, Cidade Universitária, Recife, PE, Brasil.

^cUniversidade Federal de Pernambuco, Departamento de Engenharia Química, Avenida Professor Arthur Sá, 50740-521, Cidade Universitária, Recife, PE, Brasil.

Received: December 18, 2023; Revised: March 11, 2024; Accepted: April 11, 2024

A metallic surface can exhibit low wettability through the formation of a rough structure with micro/nanometric dimensions combined with a surface energy-reducing agent. When the contact and sliding angles are $\geq 150^\circ$ and $\leq 10^\circ$, respectively, the surface is classified as superhydrophobic (SHS). The study aimed to electrodeposit a microstructure with micronanometric roughness of nickel, stearic acid (Al/Ni-SA), and nickel, stearic acid with multi-layered carbon nanotubes (Al/Ni-SA-MWCNT) on aeronautical aluminum 7050. The obtained contact angles were close to 160° , and sliding angles were less than 1° , characterizing the superhydrophobic and self-cleaning nature. Freezing tests were conducted, and the deposit with MWCNT showed longer freezing times at -22°C . The Al/Ni-SA-MWCNT condition also exhibited the best corrosion resistance with corrosion current superior by two orders of magnitude compared to the Al/Ni-Sa condition. The coatings demonstrated impressive performance, achieving corrosion inhibition efficiencies close to 100%.

Keywords: Superhydrophobicity, AA7050, MWCNT, Ice-resistant, Nickel stearate, Aeronautical.

1. Introduction

The natural world provides an extensive field of study, accessible to all for exploration and harnessing its numerous benefits. The structure of the lotus leaf and its ability to repel water, for instance, have been subjects of extensive research. The phenomenon associated with the water-repellent capability of the lotus leaf surface is termed the “Lotus Effect,” resulting in the self-cleaning property, allowing the leaf to stay clean even in polluted environments that could harm the plant’s metabolism. Subsequently, this phenomenon has been observed in bird feathers and wings of certain butterfly species. This effect is characterized by contact angles (CA) $\geq 150^\circ$ and low sliding angles (SA) $\leq 10^\circ$, inspiring the study of superhydrophobic surfaces (SHS).

In addition to self-cleaning, SHS also exhibit properties such as corrosion resistance¹, anti-freezing², anti-fogging³, anti-reflective⁴, anti-biofouling^{5,6}, drag reduction, and find applications in various sectors such as urban transport, energy, food, construction, medicine, textiles, and aerospace^{1,7}.

The formation of ice occurs on all exposed parts of an aircraft, not only limited to wings, windshields, or turbines but also in areas inaccessible to heating systems, resulting in additional challenges. For instance, ice on antennas can

induce excessive vibrations leading to breakage, while the presence of ice on control surfaces poses a challenge during flight⁸. Additionally, ice can cause errors in crucial instrument readings, such as the Pitot tube responsible for indicating airspeed^{2,9}

Aircraft, especially light ones, face the risk of reduced lift at high speeds and lower-than-normal angles of attack, along with the possibility of uncontrolled rotation and oscillation, making recovery an impossible task¹⁰. This phenomenon arises from the synergistic interaction between two main factors: surface energy-reducing agents (SERA) and a simultaneous hierarchical structure of micrometric and nanometric dimensions^{11,12}.

Additionally, water repellency can be applied to aircraft windshields and windows, sensors, and cameras to prevent fogging and water droplet formation during flight³. Superhydrophobic coatings reduce fogging by increasing the evaporation rate^{6,13,14}.

Corrosion protection is also crucial in the aerospace sector, where aircraft are exposed to aggressive environments such as humidity and various chemicals present in the atmosphere. The hierarchical structure of SHS minimizes medium contact with the substrate, significantly reducing the action of liquids or moisture^{1,15,16}.

*e-mail: jedaia.januario@ufpe.br

SERA is typically composed of a hydrophobic chain, with long-chain organic acids and silanes standing out¹⁷⁻¹⁹. They interact with the surface, forming a layer or coating that alters the surface energy, creating a barrier to surface wetting by water²⁰⁻²².

Electrodeposition stands out as a widely used process in various industries due to its speed, simplicity, and favorable cost-benefit ratio. This method allows the deposition of a variety of elements, such as nickel, gold, silver, platinum, tin, oxides, nanoparticles, among others, with the choice of metal and its precursor determined by the desired properties^{23,24}. A notable advantage of electrodeposition over other processes is the simultaneous achievement of hierarchical structure and surface energy reduction in a single step^{7,12,25}.

The inherent low surface tension of electrodeposition enables the formation of highly cohesive spherical drops, reducing the contact area with the surface. Associated with this low surface tension, the surface structure, containing micrometric and nanometric dimensions simultaneously, prevents the drop from spreading or completely wetting the surface, resulting in a rolling behavior on the surface^{26,27}.

By integrating a hierarchical structure with surface energy-reducing agents (SERA), it is possible to achieve a superhydrophobic surface (SHS). Among the SERA commonly employed are perfluoroalkylated agents (PFAS), silanes, and fatty acids. PFAS and silanes are more expensive than fatty acids, and may contain fluorine in their composition, rendering them harmful to the environment and even to human health²⁸⁻³¹. Fatty acids, on the other hand, are low-cost, easy to apply, and biodegradable^{8,32,33}. Therefore, stearic acid was chosen as the SERA instead of the others.

Methods for obtaining a superhydrophobic surface can occur in a single step or multiple steps. In the single-step process, the hierarchical structure and surface energy reduction are acquired simultaneously. The multi-step process, often described by various authors, involves the creation of a micrometric structure, the addition of a nanometric structure, and the reduction of surface energy^{12,25,32}.

In this study, two types of electrodeposited coatings were developed on the aerospace aluminum alloy AA7050. Both used nickel chloride hexahydrate (200 g/L) and stearic acid (28.4 g/L) as precursors in an alcoholic medium, with one of them reinforced with multi-walled carbon nanotubes (0.1 g/L)³⁴. Xu et al.²² previously developed a superhydrophobic coating on aluminum AA 6061 in a single step, using a solution of nickel nitrate hexahydrate and stearic acid. These coatings exhibited superhydrophobic characteristics, with contact angles of 160° and sliding angles of 2.1°, indicating an SHS. The hierarchical structure obtained on the surface resembles a cauliflower, containing both micro and nanometric dimensions. Researchers assessed corrosion resistance concerning the substrate, noting a significant increase in resistance, with values over 280 times compared to the aluminum substrate, as determined by polarization curve tests.

Soleimangoli et al.³⁵ conducted the preparation of superhydrophobic nickel coatings in two steps of electrodeposition on a copper substrate. After the first electrodeposition step, the topography took on a polyhedral shape. Subsequently, in the second electrodeposition step, using the crystallographic modifier ammonium chloride (NH₄Cl) with a concentration of 400 g/L, the structure acquired a more conical configuration,

reaching a contact angle (CA) of 155°. Corrosion resistance was evaluated for coatings with different concentrations of the crystallographic modifier, revealing that electrochemical tests demonstrated a reduction in current density by up to three orders of magnitude compared to the copper substrate.

The typical morphology of nickel electrodeposits is described by several researchers as a structure resembling cauliflower³⁶⁻³⁸. Similar to cauliflower florets, nickel electrodeposits exhibit a branched and three-dimensional structure, where multi-walled carbon nanotubes (MWCNTs) disperse in the nickel matrix, creating a complex structure³⁷.

Nickel coatings reinforced with carbon nanotubes (CNTs) have been the subject of studies due to the search for enhanced corrosion protection properties³⁹⁻⁴². The use of carbon nanotubes is widely explored due to their remarkable mechanical properties^{43,44} and electrical conductivity⁴⁵.

The incorporation of carbon nanotubes (CNTs) can have a significant influence on improving adhesion and nucleation, modifying coating growth characteristics, morphology, and structure, as well as on electrochemical behavior and interfacial interactions^{37,46,47}.

There are essentially two types of carbon nanotubes (CNTs): single-walled carbon nanotubes (SWCNTs) and multi-walled carbon nanotubes (MWCNTs). The cost associated with manufacturing SWCNTs can make this material less attractive for various applications, as the price per gram of this material is around \$700. In contrast, the production cost of MWCNTs is significantly more affordable, ranging around \$30, with the potential to vary between \$10 and \$20 per kilogram. Moreover, the properties of MWCNTs are widely considered ideal for various engineering applications⁴⁸.

Considering this information, this study proposes the development of coatings applied to the aerospace aluminum alloy 7050, using nickel nanocomposites and nickel reinforced with multi-walled carbon nanotubes. The design of these coatings will aim to confer superhydrophobic and self-cleaning characteristics, with the intention of enhancing corrosion resistance properties and mitigating ice formation on the mentioned alloy. The central objective is to contribute to the evolution of coating technologies in the aerospace industry, promoting the extension of component lifespan and raising safety standards in operations.

2. Materials and Methods

2.1. Materials

Test specimens were produced using the 7050 aluminum alloy, with dimensions of 12 × 11 × 8 millimeters. The employed precursors included absolute ethyl alcohol (99.5% PA) supplied by Anidrol Produtos para Laboratórios Ltda., stearic acid from Dinâmica Química Contemporânea Ltda., and hexahydrated nickel chloride from NEON Reagentes Analíticos Ltda. The multi-layered carbon nanotubes used in this research were obtained from the supplier Advanced 2D Materials CO., with a purity of 95%.

2.2. Surface preparation and electroplating parameters

The samples underwent a grinding process using silicon carbide (SiC) sandpapers with sequential grit sizes of

#400, #600, #800, and #1000. Subsequently, the samples were subjected to an ultrasonic bath in isopropyl alcohol for 2 minutes to remove potential impurities. Finally, to eliminate the oxide layer and activate the surface, an 8-step procedure was employed, as described by Xu et al.²², as illustrated in Figure 1.

Upon completion of the surface cleaning and activation procedure, the samples were immediately immersed in alcoholic electrolytic baths^{34,49}, based on the studies of Jena et al.⁵⁰ and Chen et al.⁵¹, as detailed in Table 1, aiming to prevent the formation of the aluminum oxide layer and achieve the super-hydrophobic characteristic of the coating. The electrodeposition process employed was potentiostatic, maintaining a constant voltage, as recommended by Yang et al.²⁵.

2.3. Morphological and compositional analysis

The morphological evaluation of the coating surface was conducted using Scanning Electron Microscopy (SEM). For chemical composition characterization, analytical techniques such as Energy-Dispersive X-ray Spectroscopy (EDS) and Energy-Dispersive X-ray Fluorescence Spectrometry (EDXRF) were employed. The SEM used was the TESCAN MIRA 3, with magnifications ranging from 1,000 to 100,000 times, and the EDS module coupled to the SEM from Oxford Instruments, model INCA X-Act.

Fourier Transform Infrared Spectroscopy (FTIR) was applied to identify the functional groups present in the surface energy reducing agent (ARS) incorporated into the coating. Jasco equipment, model FT/IR-4600, was used for this purpose. The associated software was Spectra Manager

Version 2. The wavelength range applied in the analyses was from 4000 to 500 cm^{-1} , with a resolution of 4 cm^{-1} , using a TGS detector and a scanning speed of 2 mm/s .

2.4. The wetting study

The contact angles (CA) and sliding angles (SA) were determined using the Biolin Scientific - Attension Theta Optical Tensiometer, with the OneAttension 3.0 program as the interface. The CA and SA values presented in this study were obtained by averaging three random measurements taken on the coating surface. All measurements were conducted at room temperature, employing a 10 μL drop of a distilled water deposited onto the surface⁷ according to the standard ASTM D7490-13. Additionally, surface adhesion tests were conducted, with a drop of a distilled water solution with methylene blue for easy visualization solution carefully approached to the surface. Furthermore, self-cleaning tests were performed, where gypsum powder was deposited on the coating. Considering the presence of dirt, drops were poured onto the powder, verifying the self-cleaning characteristics of the coating inclined at 5°.

2.5. Linear polarization tests

The corrosion evaluation of the samples was conducted through electrochemical tests which were developed based on the studies of Malta et al.⁵² and Xu et al.²². The linear polarization tests, carried out at room temperature, using a 3.5% NaCl aqueous solution as the corrosive medium. The electrochemical cell employed consisted of three electrodes: a working electrode (aluminum alloy sample

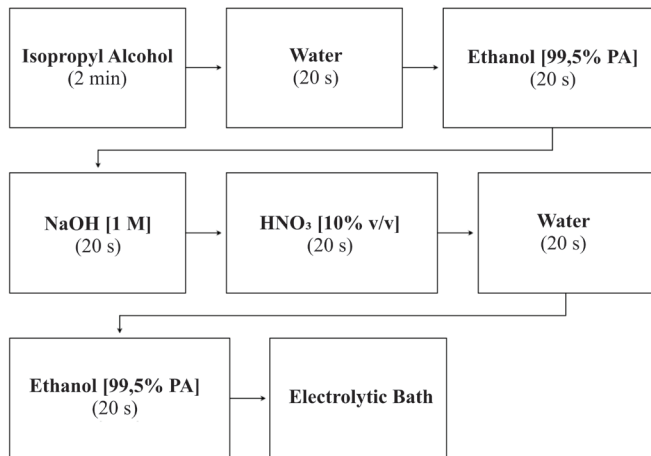


Figure 1. Flowchart of the cleaning and surface activation process for the aluminum substrate.

Table 1. Concentration of reagents and parameters used in the electrochemical baths.

Reagents	Conditions and concentrations of the precursors (g/L)			Parameter	Value
	Al	Al/Ni-SA	Al/Ni-SA-MWCNT	Temperature [°C]	25° ± 5
NiCl ₂ ·6H ₂ O (Hexahydrated nickel chloride)	-	19	19	Time [s]	300
C ₁₈ H ₃₆ O ₂ (Stearic acid)	-	28.4	28.4	Electrode gap [mm]	15
MWCNT (Multiple-walled carbon nanotubes)	-	-	0.1	DC Voltage [v]	30

with 0.96 cm² area), a platinum counter electrode, and a saturated calomel reference electrode (SCE).

The linear polarization (LP) test was performed in a potentiodynamic mode, with a scan rate of 0.001 V/s and a potential variation from -0.5 to 0.5 V from the corrosion potential obtained after 1.0h of immersion, maintaining ambient temperature conditions. Each electrochemical test was repeated three times to ensure a good reproducibility.

2.6. Ice formation resistance

The evaluation of ice formation resistance was conducted in a freezer with precise temperature control, model DFN52 from Eletrolux do Brasil S.A. Fixed intervals ranging from 0 to 12 minutes were considered. In order to facilitate the visualization of the freezing of the distilled water droplet (10 μ L), a very diluted solution with methylene blue pigment was used. The established working temperature for the experiments was -22.0°C.

3. Results and Discussions

3.1. Morphology and hierarchical structure created on aluminum 7050

The initially sanded samples up to the #1000 grit size, as shown in Figures 2A.1 and 2A.2, display the characteristic sanding marks of the aluminum 7050 substrate before the electrodeposition process, highlighted by yellow arrows. In Figures 2B and 2C, sanding marks are no longer observed, demonstrating the surface modification through coating deposition. It is noted that the Al/Ni-SA condition, shown in Figure 2B, presents itself as a rough and porous coating with the morphology of small cauliflower-like branches at micro-nano scale.

Analyzing the coating condition Al/Ni-SA-MWCNT, Figures 2C.1 and 2C.2 corresponding to the nickel coatings containing both stearic acid and MWCNT applied respectively

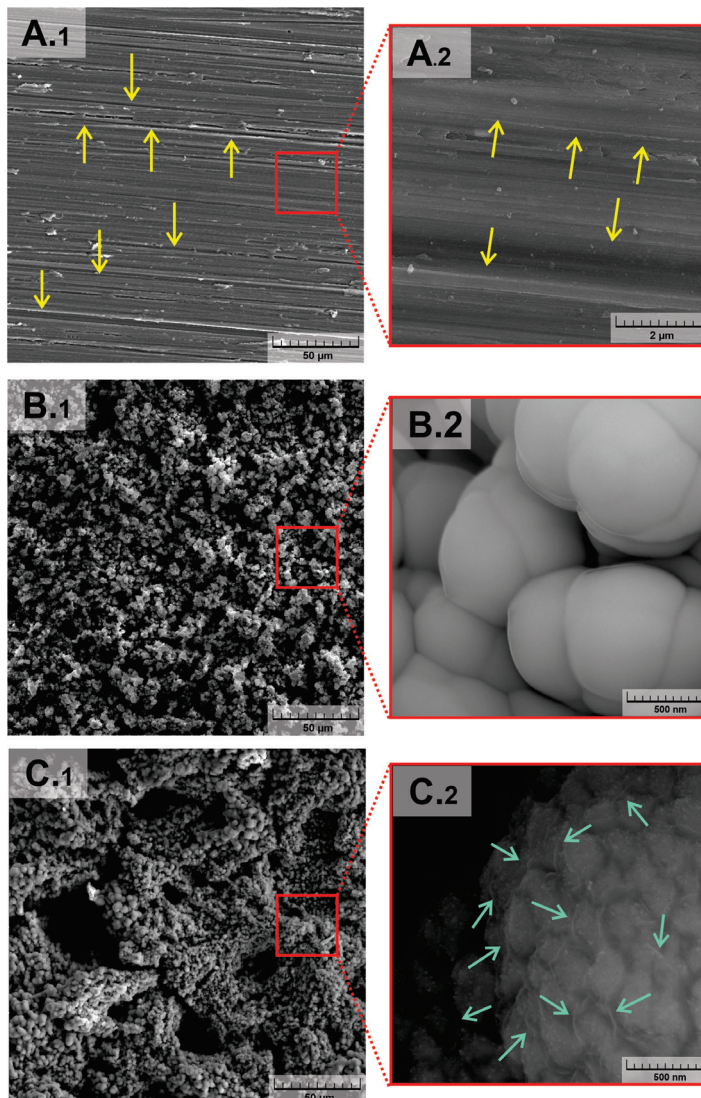


Figure 2. SEM images of the topography of the studied conditions with different magnifications. (A) Surface of AA7050 after the sanding process and conditions (B) Al/Ni-SA and (C) Al/Ni-SA-MWCNT.

on the aluminum alloy substrate, it can be observed that there is the formation of nanoparticulate deposits in both cases, forming even larger clusters than the previously mentioned condition. Additionally, in Figure 2C.2, at the nanoscale, structures resembling carbon nanotubes incorporated into the coating during the electrodeposition process can be seen, highlighted by cyan arrows.

The formation of micro-nanostructured hierarchies associated with surface energy-reducing agents such as stearic acid may promote the formation of air pockets that prevent water access from the substrate, achieving high water repellency, as demonstrated in studies conducted by Xu et al.²², Shen et al.⁵³, and Chen et al.⁵¹.

According to Guo et al.²⁰ and Kararlioglu and Akbulut⁴⁷, MWCNTs in solution can act as nucleation facilitators for nickel due to their thin shape and high electrical conductivity. Thus, reduced nickel and nickel stearate can be more easily incorporated in the coating. This behavior is evident from the protrusions of the coatings present in the conditions.

As observed, the alloying elements identified for the aluminum alloy 7050 were Zn, Cu, Mg, and Si, Table 2, consistent with findings by Vargel⁵⁴ and Dursun⁵⁵.

The analysis of the EDS spectra, Figure 3, showed that the conditions Al/Ni-SA and Al/Ni-SA-MWCNT presented peaks related to the elements present in the reagents used during the electrochemical bath, confirming the incorporation of these elements into the deposit. However, for the Al/Ni-SA condition, the presence of aluminum was evidenced, even in small quantities, indicating the existence of pores and/or other defects in the coating. On the other hand, for the Al/Ni-SA-MWCNT deposit, the absence of the aluminum peak suggests a more efficient coverage of the substrate, preventing exposure of the aluminum alloying elements. As presented earlier in Figures 2B.1 and 2C.1, coatings under these conditions showed more voluminous coatings with overlapping layers.

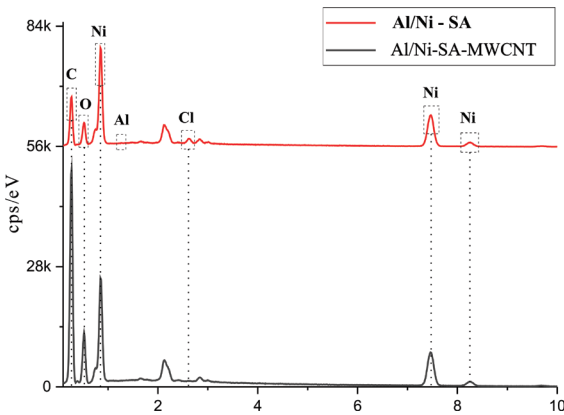


Figure 3. Compositional analysis by EDS of the nickel-deposited coatings.

The FTIR technique generated the same spectrum for both studied conditions. There are three highlighted regions in the graph, Figure 4, which are the peak characterized by the wavenumber 2953 cm^{-1} , corresponding to the stretching vibration of the methyl group ($-\text{CH}_3$)²², stretching and bending vibrations of the ($-\text{CH}_2$) group bonds²² can be seen around the peaks 2914 and 2846 cm^{-1} . Another prominent region is the stretching band around the peaks 1538 and 1402 cm^{-1} associated with the carboxylate functional group ($-\text{O}-\text{C}=\text{O}$). The absence of a peak at 1700 cm^{-1} , associated with the $-\text{COOH}$ group, and the strong presence of the peak related to the carboxylate group suggest that stearic acid molecules reacted with nickel and formed a nickel stearate ionic complex incorporated into the coating⁵⁶.

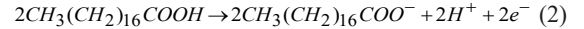
3.2. Mechanism of superhydrophobic surface formation (SHS)

The electrodeposition mechanism occurs in accordance with the following steps, as depicted in Figure 5.

- I. Reduction of nickel ions: The nickel ions in the solution are reduced and deposit on the cathode surface along with carbon nanotubes, as shown in Equation 1.



- II. Oxidation of stearic acid: Stearic acid loses two electrons, releasing hydrogen ions, carboxylate, and electrons, as represented by Equation 2.



- III. The carboxylate anions combine with the nickel cation present in the solution, forming nickel

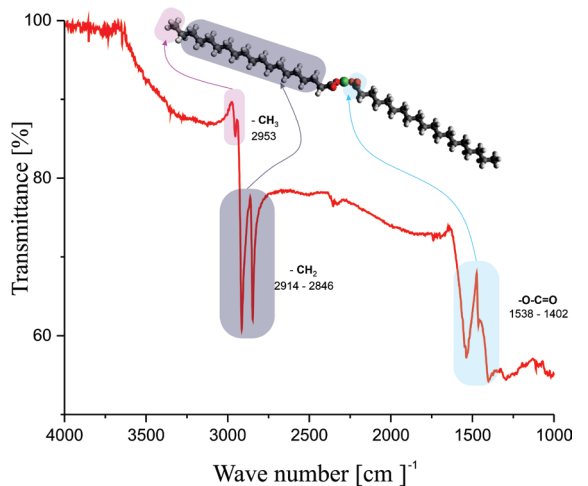
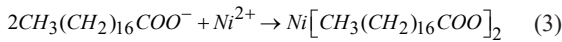


Figure 4. FT-IR spectrum of the SHS samples showing the functional groups present in the coating.

Table 2. Compositional analysis by EDXRF of the aluminum 7050 substrate.

	Al	Mg	Si	S	Fe	Ni	Cu	Zn	Sn
(%)	92,730	2,328	0.138	0.022	0.084	0.002	1,689	3,005	0.001

carboxylate or nickel stearate, as demonstrated by Equation 3.



- IV. The hydrogen present in the solution also undergoes reduction to form gaseous hydrogen. This reaction is known as hydrogen evolution and is presented in Equation 4.



- V. The carbon nanotubes in the Al/Ni-SA-MWCNT solution act as facilitators for the nucleation of metallic nickel due to their thin shape and good electrical conductivity. Therefore, in the solution, nickel will be reduced onto the carbon nanotubes^{20,47}.

3.3. Wettability, self-cleaning, and surface adhesion

Stearic acid plays the role of an efficient Surface Energy Reducing Agent (SERA). Due to its long polar carbon chain, it contributes to the hydrophobic nature of the surface. Additionally, the morphology with micro and nanoscale roughness traps air, enhancing water repellency. The synergistic effect between micro-nano roughness and SERA promotes the super-hydrophobic property of the surface through the formation of nickel stearate.

The initial aluminum substrate initially exhibits a contact angle of $15.4^\circ \pm 0.1^\circ$, with a sliding angle greater than 10° ,

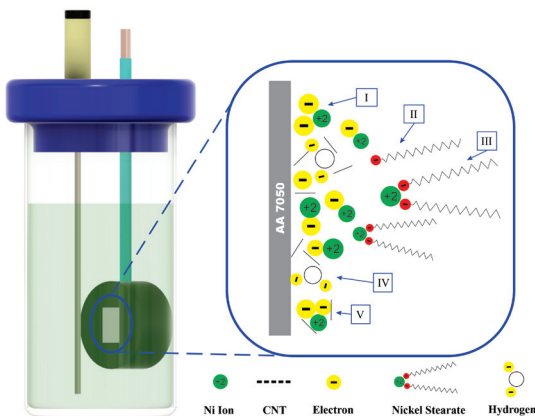


Figure 5. Representation of the nickel electrodeposition mechanism described in steps I to V.

classifying it as hydrophilic (Figure 6A). On the other hand, the Al/Ni-SA and Al/Ni-SA-MWCNT conditions obtained contact angle values of $153.3^\circ \pm 3.9^\circ$ and $154.3^\circ \pm 3.0^\circ$, with sliding angles less than $1^\circ \pm 1^\circ$, classifying them as super-hydrophobic (Figures 6B and 6C).

When slowly approaching the droplet to the aluminum surface, it is observed that it adheres to the surface. This occurs due to the higher surface energy of aluminum compared to the bonding energy of the water solution with methylene blue, as illustrated in Figure 7A. Under other conditions, a distinct behavior is observed, where the droplet does not adhere to the surface. This effect is attributed to the presence of stearic acid and surface roughness, which kept the surface energy lower than the bonding energy of water molecules.

The high contact angles and low sliding angles in the Al/Ni-SA and Al/Ni-SA-MWCNT conditions are related to the adhesiveness of the droplet to the surface, as illustrated in Figures 7A and 7B. The higher the contact angle, the lower the adhesion of the liquid to the surface. Therefore, if the surface is super-hydrophobic, the contact angle of the liquid droplet will be high, indicating that the droplet does not adhere to the surface.

Furthermore, the droplet was easily separated from the super-hydrophobic surface without leaving any visible residue, and the water droplet even diverted to the side of the needle during the deformation process, demonstrating the low adhesion of the surface⁵⁷. The self-cleaning nature of a surface is characterized by the fact that, when a drop comes into contact with the surface, it incorporates dirt and rolls, carrying with it the particulates present on the surface, as described in Figure 8A below. A surface that does not have a self-cleaning character, the drop slides over the surface, but does not take dirt with it, Figure 8B.

When the drop hits the aluminum surface, it spreads over the dirt or surface, but does not roll off, causing the particulates to remain on the test piece. This occurs because the surface energy of aluminum is greater than the bond energy of the water solution with methylene blue, Figure 9A.

On the other hand, on the self-cleaning superhydrophobic surface, the adhesion between the dirt and the surface is weaker than that between the water droplet and the dirt. This occurs because the superhydrophobic surface has a high contact angle with the water, which means that the water droplet does not adhere to the surface, as seen in Figure 9B and Figure 9C.

3.4. Freezing test

The freezing time was recorded under all conditions to assess the influence of surface roughness on this process.

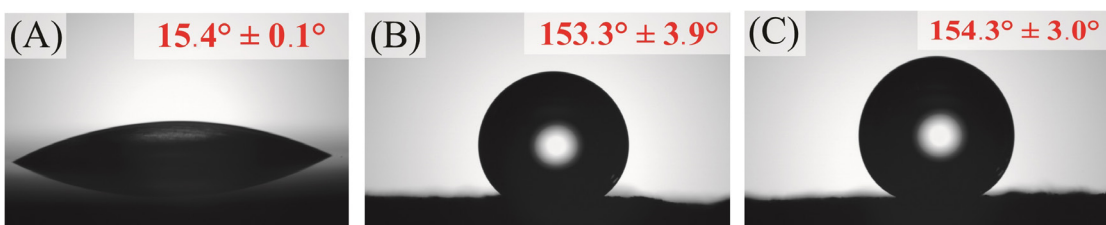


Figure 6. Surface contact angles of the (A) uncoated surface, and coated surfaces under the conditions (B) Al/Ni-SA and (C) Al/Ni-SA-MWCNT.

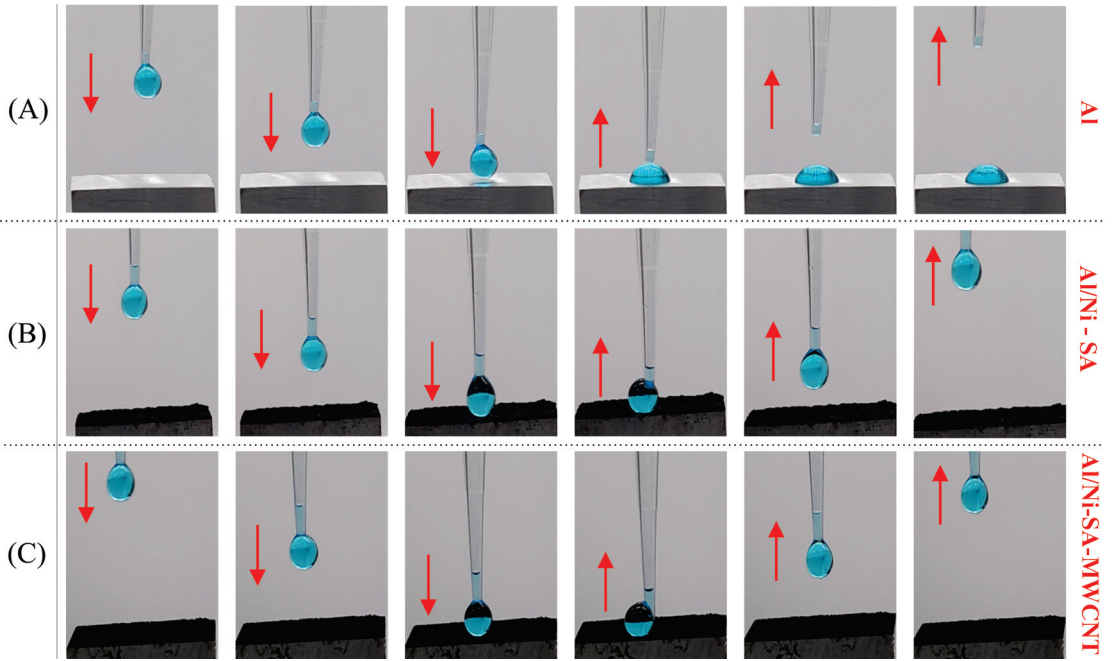


Figure 7. Adhesion test of the (A) hydrophilic condition and (B), (C) super-hydrophobic conditions.

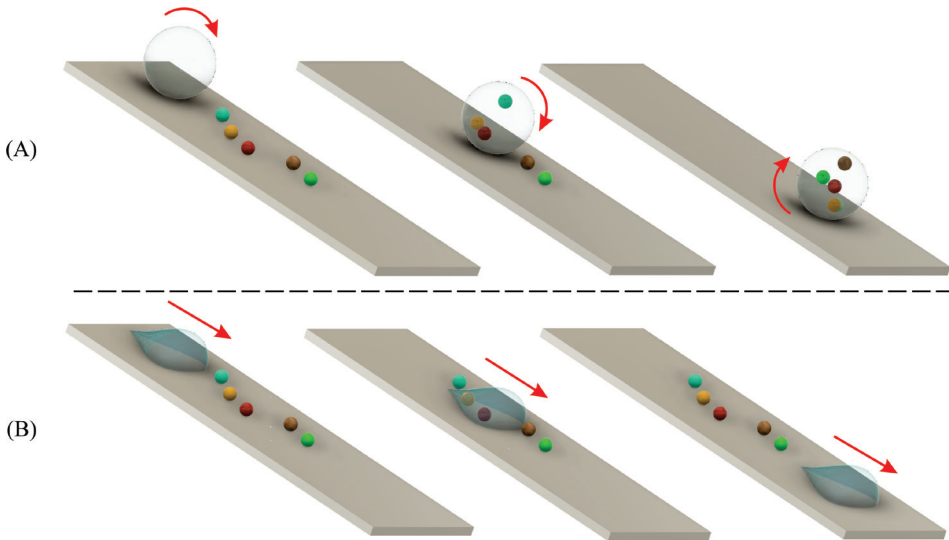


Figure 8. Surfaces (A) with or (B) without self-cleaning characteristics.

The onset of freezing was marked by the change in color of the droplet and an increase in opacity, as illustrated in Figure 10. For the Al condition, the droplet was completely frozen in 360 seconds, for Al/Ni-SA, 480 seconds, and for Al/Ni-SA-MWCNT, 720 seconds.

On smoother surfaces, the contact area is larger, maximizing thermal conduction and resulting in faster freezing. On the other hand, a droplet deposited on a surface in the Cassie-Baxter regime experiences increased freezing time due to the trapped air beneath the droplet, reducing surface contact with the liquid phase. Additionally,

air, being a poor thermal conductor, along with surface roughness, hinders heat transfer between the surface and the liquid⁵⁸.

The presence of carbon nanotubes incorporated into the Al/Ni-SA-MWCNT coating resulted in a more compact and rough coating, prolonging the freezing time by about two times compared to the aluminum substrate.

3.5. Analysis of anticorrosive properties

Through the intersection of the cathodic and anodic Tafel curves, as shown in Figure 11, the pairs (E_{corr} and i_{corr})

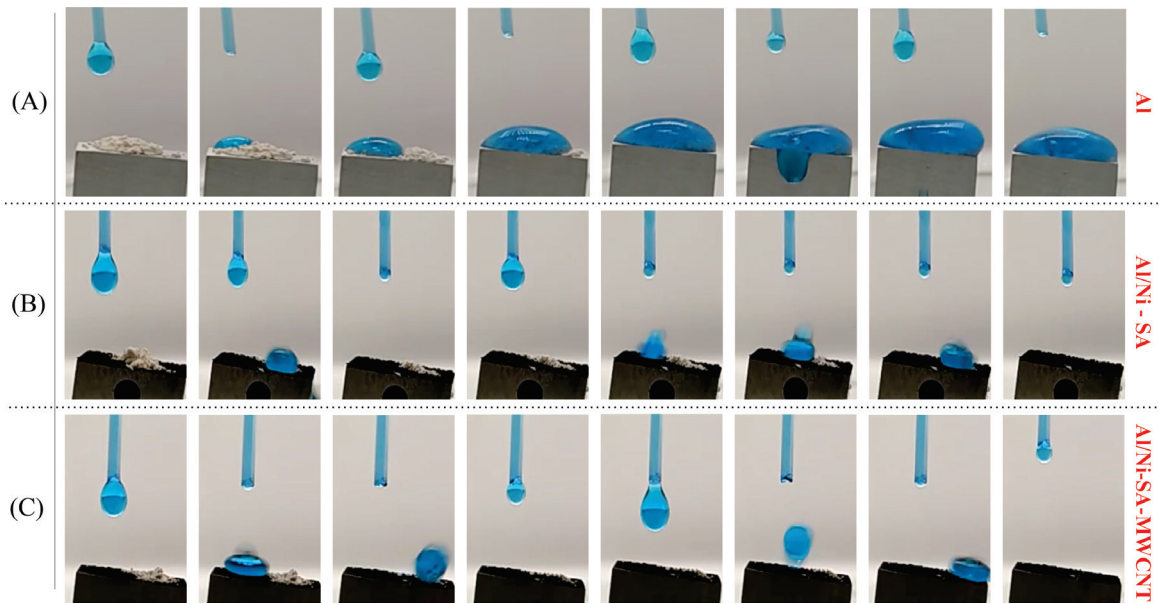


Figure 9. Self-cleaning tests of the conditions (A) Al (B) Al/Ni-SA and (C) Al/Ni-SA-MWCNT.

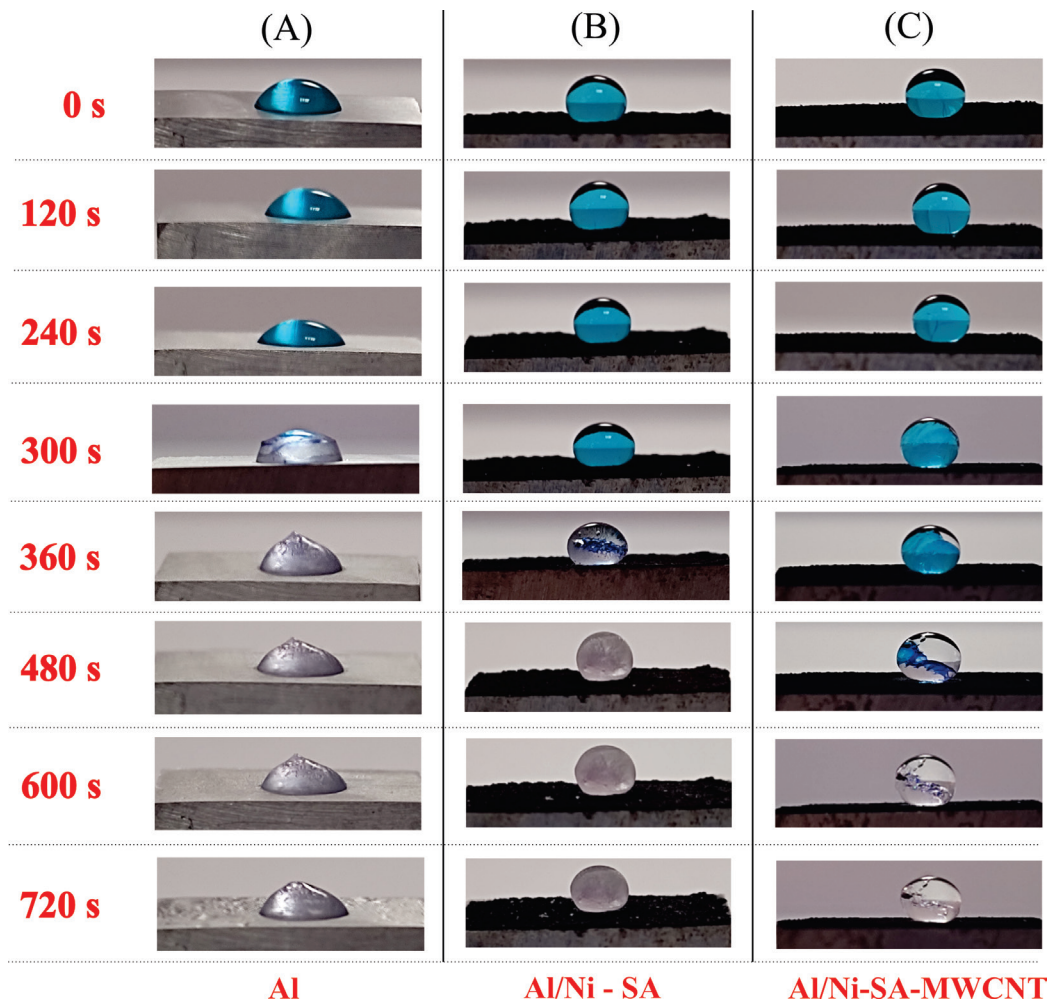


Figure 10. Variation of freezing times for each condition.

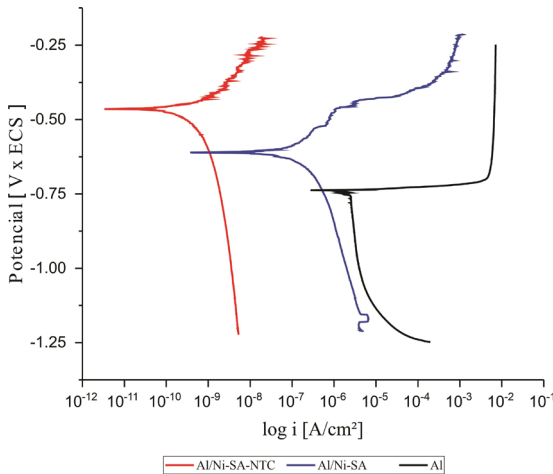


Figure 11. Polarization tests for the uncoated and coated condition.

Table 3. Corrosion potential and corrosion current results.

Condition	E_{corr} [v]	I_{corr} [A/cm^2]
Al	-0.737	$2,1984 \times 10^{-6}$
Al/Ni-SA	-0.613	$7,4282 \times 10^{-8}$
Al/Ni-SA-MWCNT	-0.465	$1,7713 \times 10^{-10}$

were obtained for each studied condition. These values are detailed in Table 3.

The Al/Ni-SA-MWCNT condition showed the best performance in corrosion resistance, with E_{corr} values of -0.465 V and i_{corr} of 1.7713×10^{-10} A/cm². The corrosion current was two orders of magnitude higher than that of the Al/Ni-SA condition. This improvement can be attributed to the presence of NTCPM, which potentiated the formation of nickel stearate, giving the coating a super-hydrophobic character and thus hindering electrolyte access to the substrate.

Furthermore, the inhibition efficiency of SSHS coatings was calculated using Equation 5³⁸:

$$\eta = \frac{(i_{corr/subs} - i_{corr/SHF})}{i_{corr/subs}} \times 100\% \quad (5)$$

Where $i_{corr/subs}$ and $i_{corr/SHS}$ are the corrosion currents of the substrate and the SHS surface, respectively.

The calculated efficiencies revealed corrosion efficiencies of 96.6% and 99.9% for the Al/Ni-SA and Al/Ni-SA-MWCNT conditions after 24 hours of exposure to the saline medium, respectively. These values were higher than those found by Yin et al.⁵⁹ (96.0%), Su et al.⁶⁰ (91.9%), Wan et al.⁶¹ (97.8%), and Malta et al.⁵² (76.9%) for the same saline medium.

4. Conclusions

At the end of the experiments, it was possible to highlight that:

- Superhydrophobic coatings on 7050 aluminum alloy with self-cleaning property were obtained for all samples from a viable electrodeposition process and in a single stage, presenting hierarchical

structures on a micro- and nano-scale associated with the formation of nickel stearate.

- The sample surfaces so obtained presented similar wettability behavior. The samples with carbon nanotubes (AL/Ni-SA-MWCNT) presented a contact angle of 154.3° and without carbon nanotubes (AL/Ni-SA) 153.3°, both presented sliding angles of 1°.
- The Tafel method revealed excellent anti-corrosion properties, with inhibition efficiency results of 96.6% and 99.9% for AL/Ni-SA and AL/Ni-SA-MWCNT, respectively, after 24 hours of exposure in 0.6 mol/L NaCl solution.
- Additionally, these coating surfaces have exhibited non-adherence to water during adhesion tests, as well as better resistance to ice formation, with freezing time values of 480s for AL/Ni-SA and 720s for AL/Ni-SA-MWCNT.
- The presence of nanotubes influenced the final properties of the coating, presenting better results in wettability, inhibition corrosion efficiency, and resistance to ice formation, all due to the favoring of nickel stearate nucleation by MWCNT conductive particles.

5. Acknowledgments

This research was performed at the Federal University of Pernambuco/Brazil by the National Institute of Technology in Union and Materials Coating (INTM), Laboratory of Composite Materials and Structural Integrity (LBC-Compolab) and Research Institute in Petroleum and Energy (LITPEG). This work has been supported by the National Council of Scientific and Technological Development (CNPq/Brazil) (n° 409725/2023-4); Folks Improvement Coordination of Higher Education (CAPES); Financier of Studies and Projects (Finep); National Agency for Petroleum and Natural Gas and Biofuels (ANP). The authors would like to express their sincere gratitude for the financial grant from the Support Foundation for Science (FACEPE).

6. References

1. Shi T, Liang J, Li X, Zhang C, Yang H. Improving the corrosion resistance of aluminum alloy by creating a superhydrophobic surface structure through a two-step process of etching followed by polymer modification. *Polymers*. 2022;14(21):4509.
2. Hu H, Al-Masri F, Tian L, Hu H. Experimental study of dynamic icing process on a pitot probe model. *J Thermophys Heat Trans*. 2023;37(3):632.
3. Yoon J, Ryu M, Kim H, Ahn GN, Yim SJ, Kim D-P, et al. Wet-style superhydrophobic antifogging coatings for optical sensors. *Adv Mater*. 2020;32(34):2002710.
4. Isakov K, Kauppinen C, Franssila S, Lipsanen H. Superhydrophobic antireflection coating on glass using grass-like alumina and fluoropolymer. *ACS Appl Mater Interfaces*. 2020;12(44):49957-62.
5. Sahin F, Celik N, Ceylan A, Pekdemir S, Ruzi M, Onses MS. Antifouling superhydrophobic surfaces with bactericidal and SERS activity. *Chem Eng J*. 2022;431:133445. <http://doi.org/10.1016/j.cej.2021.133445>.
6. Jeevahan J, Chandrasekaran M, Joseph GB, Durairaj RB, Mageshwaran G. Superhydrophobic surfaces: a review on

- fundamentals, applications, and challenges. *J Coat Technol Res.* 2018;15(2):231-50.
7. Silva RGC, Malta MIC, Carvalho LAP, Silva JJ, Silva WLC Fo, Oliveira SH, et al. Low-cost superhydrophobic coating on aluminum alloy with self-cleaning and repellency to water-based mixed liquids for anti-corrosive applications. *Surf Coat Tech.* 2023;457:129293. <http://doi.org/10.1016/j.surfcoat.2023.129293>.
 8. Li H, Chen Y, Jakobs U. Synthesis, control, and excitation of characteristic modes for platform-integrated antenna designs: a design philosophy. *IEEE Antennas Propag Mag.* 2022;64(2):41-8.
 9. Lin Y, Chen H, Wang G, Liu A. Recent progress in preparation and anti-icing applications of superhydrophobic coatings. *Coatings.* 2018;8(6):208.
 10. Baars WJ, Stearman RO, Tinney CE. A review on the impact of icing on aircraft stability and control. *J Aero Struct Dyn.* 2010;2(1):35-52.
 11. Miller RH, Hu S, Weamie SJ, Naame SA, Kiazolu DG. Superhydrophobic coating fabrication for metal protection based on electrodeposition application: a review. *J Mater Sci Chem Eng.* 2021;9(4):68-104. <http://doi.org/10.4236/msce.2021.94008>.
 12. Khan MZ, Militky J, Petru M, Tomková B, Ali A, Tören E, et al. Recent advances in superhydrophobic surfaces for practical applications: a review. *Eur Polym J.* 2022;178:111481.
 13. Nyankson E, Agbe H, Takyi GKS, Bensah YD, Sarkar DK. Recent advances in nanostructured superhydrophobic surfaces: fabrication and long-term durability challenges. *Curr Opin Chem Eng.* 2022;36:100790.
 14. Bai Y, Zhang H, Shao Y, Zhang H, Zhu J. Recent progresses of superhydrophobic coatings in different application fields: an overview. *Coatings.* 2021;11(2):116.
 15. Gupta R, Verma R, Kango S, Constantin A, Kharia P, Saini R, et al. A critical review on recent progress, open challenges, and applications of corrosion-resistant superhydrophobic coating. *Mater Today Commun.* 2023;34:105201.
 16. Jin Z, Mei H, Pan L, Liu H, Cheng L. Superhydrophobic self-cleaning hierarchical micro-/nanocomposite coating with high corrosion resistance and durability. *ACS Sustain Chem& Eng.* 2021;9(11):4111-21.
 17. Torun I, Celik N, Ruzi M, Onses MS. Transferring the structure of paper for mechanically durable superhydrophobic surfaces. *Surf Coat Tech.* 2021;405:126543.
 18. Nguyen-Tri P, Tran HN, Plamondon CO, Tuduri L, Vo DVN, Nanda S, et al. Recent progress in the preparation, properties and applications of superhydrophobic nano-based coatings and surfaces: a review. *Prog Org Coat.* 2019;132:235-56.
 19. Zhang X, Shi F, Niu J, Jiang Y, Wang Z. Superhydrophobic surfaces: from structural control to functional application. *J Mater Chem.* 2008;18(6):621-33.
 20. Guo Y, Li C, Li X, Xu H, Chen W, Fang K, et al. Fabrication of superhydrophobic cotton fabric with multiple durability and wearing comfort via an environmentally friendly spraying method. *Ind Crops Prod.* 2023;194:116359.
 21. Rabbani S, Bakshshandeh E, Jafari R, Momen G. Superhydrophobic and icephobic polyurethane coatings: fundamentals, progress, challenges and opportunities. *Prog Org Coat.* 2022;165:106715.
 22. Xu N, Sarkar DK, Chen XG, Tong WP. Corrosion performance of superhydrophobic nickel stearate/nickel hydroxide thin films on aluminum alloy by a simple one-step electrodeposition process. *Surf Coat Tech.* 2016;302:173-84.
 23. Pu SD, Gong C, Tang YT, Ning Z, Liu J, Zhang S, et al. Achieving ultrahigh-rate planar and dendrite-free zinc electroplating for aqueous zinc battery anodes. *Adv Mater.* 2022;34(28):2202552.
 24. Satpathy B, Jena S, Das S, Das K. A comprehensive review of various non-cyanide electroplating baths for the production of silver and gold coatings. *Int Mater Rev.* 2023;68(7):825-61.
 25. Yang Z, Liu X, Tian Y. Fabrication of super-hydrophobic nickel film on copper substrate with improved corrosion inhibition by electrodeposition process. *Colloids Surf A Physicochem Eng Asp.* 2019;560:205-12.
 26. Hooda A, Goyat MS, Pandey JK, Kumar A, Gupta R. A review on fundamentals, constraints and fabrication techniques of superhydrophobic coatings. *Prog Org Coat.* 2020;142:105557.
 27. Crawford RJ, Ivanova EP. *Superhydrophobic surfaces.* Amsterdam: Elsevier; 2015.
 28. Mohseni M, Lahiri SK, Nadaraja AV, Sundararaj U, Golovin K. Durable and comfortable superoleophobic fabrics utilizing ultra-short-chain fluorinated surface chemistry. *Chem Eng J.* 2023;471:144726.
 29. Barman T, Chen H, Liu J, Yang G, Zhao W, Peng C, et al. Synthesis and characterization of styrene-based polyfluoroacrylate film for hydrophobic/icephobic applications. *Thin Solid Films.* 2019;687:137462.
 30. Qi Y, Yang Z, Huang W, Zhang J. Robust superhydrophobic surface for anti-icing and cooling performance: application of fluorine-modified TiO₂ and fumed SiO₂. *Appl Surf Sci.* 2021;538:148131.
 31. Qi Y, Chen S, Zhang J. Fluorine modification on titanium dioxide particles: improving the anti-icing performance through a very hydrophobic surface. *Appl Surf Sci.* 2019;476:161-73.
 32. Silva RG, Vieira MR, Malta MI, Silva CH, Oliveira SH, Severino LU Fo. Effect of initial surface treatment on obtaining a superhydrophobic surface on 5052 aluminum alloy with enhanced anticorrosion properties. *Surf Coat Tech.* 2019;369:311-22.
 33. Ahmad N, Rasheed S, Ahmed K, Musharraf SG, Najam-ul-Haq M, Hussain D. Facile two-step functionalization of multifunctional superhydrophobic cotton fabric for UV-blocking, self-cleaning, antibacterial, and oil-water separation. *Separ Purif Tech.* 2023;306:122626.
 34. Prasannakumar RS, Chukwuike VI, Bhakayaraj K, Mohan S, Barik RC. Electrochemical and hydrodynamic flow characterization of corrosion protection persistence of nickel/multiwalled carbon nanotubes composite coating. *Appl Surf Sci.* 2020;507:145073.
 35. Soleimangoli F, Hosseini SA, Davoodi A, Mokhtari A, Alishahi M. Effect of NH₄Cl on the microstructure, wettability and corrosion behavior of electrodeposited Ni-Zn coatings with hierarchical nano/microstructure. *Surf Coat Tech.* 2020;394:125825.
 36. Wang J, Zhang Y, He Q. Durable and robust superhydrophobic fluororubber surface fabricated by template method with exceptional thermostability and mechanical stability. *Separ Purif Tech.* 2023;306:122423.
 37. Park JH, Hagio T, Ichino R. Improvement in the corrosion resistance of electrodeposited Ni-W alloy by NTCMP co-deposition and prevention of metal-carbon interfacial corrosion by carbide formation. *J Alloys Compd.* 2023;939:168788.
 38. Yang Z, Liu X, Tian Y. Fabrication of super-hydrophobic nickel film on copper substrate with improved corrosion inhibition by electrodeposition process. *Colloids Surf A Physicochem Eng Asp.* 2019;560:205-12.
 39. Lopes A, Banczek E, Costa I, Terada M, Cunha M, Rodrigues P. Caracterização de níquel eletrodepositado na presença de nanotubos de carbono (NTC). In: 19^o Congresso Brasileiro de Engenharia e Ciência dos Materiais (CBECiMat); 2022; Campos do Jordão, SP, Brasil. Anais. São Paulo: ABC/ABM/ABPol; 2022.
 40. Jyothender KS, Gupta A, Srivastava C. Grain boundary engineering in Ni-carbon nanotube composite coatings and its effect on the corrosion behaviour of the coatings. *Materialia.* 2020;9:100617.
 41. ShathishKumar JS, Jegan A. Assessment on the microhardness and corrosion resistance characteristics of Ni-SiC and Ni-NTCPM coatings by pulse reverse electrodeposition technique. *Mater Res Express.* 2020;7(5):055012.
 42. Carpenter CR, Shipway PH, Zhu Y. Electrodeposition of nickel-carbon nanotube nanocomposite coatings for enhanced wear resistance. *Wear.* 2011;271(9-10):2100-5.

43. Wong EW, Sheehan PE, Lieber CM. Nanobeam mechanics: elasticity, strength, and toughness of nanorods and nanotubes. *Science*. 1997;277(5334):1971-5.
44. Demczyk BG, Wang YM, Cumings J, Hetman M, Han W, Zettl A, et al. Direct mechanical measurement of the tensile strength and elastic modulus of multiwalled carbon nanotubes. *Mater Sci Eng A*. 2002;334(1-2):173-8.
45. Collins PG, Bradley K, Ishigami M, Zettl DA. Extreme oxygen sensitivity of electronic properties of carbon nanotubes. *Science*. 2000;287(5459):1801-4.
46. Nasirpour F, Alipour K, Daneshvar F, Sanaeian MR. Electrodeposition of anticorrosion nanocoatings. In: Rajendran S, Nguyen TA, Kakooei S, Yeganeh M, Li Y, editors. *Corrosion protection at the nanoscale: a volume in micro and nano technologies*. Amsterdam: Elsevier; 2020. p. 473-97. <http://doi.org/10.1016/B978-0-12-819359-4.00024-6>.
47. Karslioglu R, Akbulut H. Comparison microstructure and sliding wear properties of nickel-cobalt/CNT composite coatings by DC, PC and PRC current electrodeposition. *Appl Surf Sci*. 2015;353:615-27.
48. Su X, Wang R, Li X, Araby S, Kuan HC, Naeem M, et al. A comparative study of polymer nanocomposites containing multi-walled carbon nanotubes and graphene nanoplatelets. *Nano Mater Sci*. 2022;4(3):185-204.
49. Zhou S, Zhu X, Ma L, Yan Q, Wang S. Outstanding superhydrophobicity and corrosion resistance on carbon-based film surfaces coupled with multi-walled carbon nanotubes and nickel nano-particles. *Surf Sci*. 2018;677:193-202.
50. Jena G, Thinaharan C, George RP, Philip J. Robust nickel-reduced graphene oxide-myristic acid superhydrophobic coating on carbon steel using electrochemical codeposition and its corrosion resistance. *Surf Coat Tech*. 2020;397:125942.
51. Chen Z, Hao L, Chen A, Song Q, Chen C. A rapid one-step process for fabrication of superhydrophobic surface by electrodeposition method. *Electrochim Acta*. 2012;59:168-71.
52. Malta MIC, Vieira MRS, Silva RGCD, Silva LMCD, Araújo EGD, Maciel SHDO, et al. Superhydrophobic surfaces on 5052 aluminum alloy obtained from LDH film modified with stearic acid for enhanced corrosion protection. *Mater Res*. 2019;22(6):e20180882.
53. Shen L, Fan M, Qiu M, Jiang W, Wang Z. Superhydrophobic nickel coating fabricated by scanning electrodeposition. *Appl Surf Sci*. 2019;483:706-12.
54. Vargel C. *Corrosion of aluminium*. Amsterdam: Elsevier; 2020. <http://doi.org/10.1016/B978-0-08-099925-8.00008-9>.
55. Dursun T, Soutis C. Recent developments in advanced aircraft aluminium alloys. *Mater Des*. 2014;56:862-71.
56. Chen Z, Tian F, Hu A, Li M. A facile process for preparing superhydrophobic nickel films with stearic acid. *Surf Coat Tech*. 2013;231:88-92.
57. Wang L, Xiao X, Liu E, Yu S, Yin X, Wang J, et al. Fabrication of superhydrophobic needle-like Ca-P coating with anti-fouling and anti-corrosion properties on AZ31 magnesium alloy. *Colloids Surf A Physicochem Eng Asp*. 2021;620:126568.
58. Liu X, Zhang TC, He H, Ouyang L, Yuan S. A stearic Acid/CeO₂ bilayer coating on AZ31B magnesium alloy with superhydrophobic and self-cleaning properties for corrosion inhibition. *J Alloys Compd*. 2020;834:155210.
59. Yin Y, Liu T, Chen S, Liu T, Cheng S. Structure stability and corrosion inhibition of super-hydrophobic film on aluminum in seawater. *Appl Surf Sci*. 2008;255(5):2978-84.
60. Su H, Wang L, Wu Y, Zhang Y, Zhang J. Insight into inhibition behavior of novel ionic liquids for magnesium alloy in NaCl solution: experimental and theoretical investigation. *Corros Sci*. 2020;165:108410.
61. Wan Y, Chen M, Liu W, Shen X, Min Y, Xu Q. The research on preparation of superhydrophobic surfaces of pure copper by hydrothermal method and its corrosion resistance. *Electrochim Acta*. 2018;270:310-8.